



## RESEARCH ARTICLE

[View Article Online](#)  
[View Journal](#) | [View Issue](#)

 Cite this: *Inorg. Chem. Front.*, 2022, **9**, 4075

# Achieving a strong second harmonic generation response and a wide band gap in a Hg-based material†

 Yujie Zhang, Hongping Wu,  Zhanggui Hu, Jiyang Wang, Yicheng Wu and Hongwei Yu \*

A new Hg-based infrared nonlinear optical (IR NLO) crystal,  $[\text{Ba}_4\text{Cl}_2][\text{HgGa}_4\text{S}_{10}]$ , was synthesized based on a property-oriented structural design strategy. It crystallizes in the noncentrosymmetric tetragonal space group ( $I4$ ) and consists of a 3D  $[\text{HgGa}_4\text{S}_{10}]^{6-}$  anionic moiety formed by corner-sharing tetrahedral  $\text{HgS}_4$  and supertetrahedral  $\text{Ga}_4\text{S}_{10}$  clusters, as well as a 3D  $[\text{Ba}_4\text{Cl}_2]^{6+}$  cation network. The physical property measurements show that it can exhibit well-balanced NLO performances, including a large second-harmonic generation (SHG) response ( $1.5 \times \text{AgGaS}_2$ ), wide band gap (2.95 eV), and high laser damage threshold ( $\sim 15 \times \text{AgGaS}_2$ ). First-principles calculations indicate that the large SHG response of  $[\text{Ba}_4\text{Cl}_2][\text{HgGa}_4\text{S}_{10}]$  mainly originates from the strong covalent  $\text{HgS}_4$  and  $\text{GaS}_4$  tetrahedra and the ionic bonding  $[\text{Ba}_4\text{Cl}_2]^{6+}$  guest network contributes to the wide band gap of  $[\text{Ba}_4\text{Cl}_2][\text{HgGa}_4\text{S}_{10}]$ .

 Received 29th April 2022,  
 Accepted 12th June 2022  
 DOI: 10.1039/d2qi00937d  
[rsc.li/frontiers-inorganic](https://rsc.li/frontiers-inorganic)

Infrared nonlinear optical (IR NLO) crystals are of immense scientific and technological interest because of their capabilities of generating tunable coherent lasers in the mid-IR region (2.5–25  $\mu\text{m}$ ), which are urgently needed by numerous advanced science and technologies, such as medical treatment, atmospheric monitoring, infrared countermeasures, and laser communication.<sup>1–7</sup> Hitherto, practically used IR NLO crystals mainly consist of chalcopyrite-type  $\text{AgGaS}_2$ ,  $\text{AgGaSe}_2$ , and  $\text{ZnGeP}_2$ . Although these crystals can exhibit a wide IR transparent window and large NLO responses, the low laser-induced damage threshold of  $\text{AgGaS}_2$  and  $\text{AgGaSe}_2$ , and the unexpected multiple-photon absorptions of  $\text{ZnGeP}_2$  tremendously hinder their applications under high-power conditions.<sup>8–10</sup> Hence, it is imperative to explore new IR NLO crystals with balanced properties.

Generally, an excellent IR NLO crystal should satisfy the following crucial NLO criteria: (i) a strong phase-matching SHG response ( $d_{ij} > 0.5 \text{ AgGaS}_2$ ); (ii) a high LDT ( $> 10 \text{ AgGaS}_2$ ) and a wide band gap ( $E_g > 3.0 \text{ eV}$ ); (iii) a broad transmission region (3–12  $\mu\text{m}$ ); and (iv) good physicochemical stability. Nevertheless, it is well-known that large SHG responses mainly derive from the covalency of a compound, whereas a high

laser-induced damage threshold strongly depends on its ionicity. This implies the undesired contradiction between SHG responses and the laser-induced damage threshold.<sup>11</sup> Therefore, achieving large SHG responses and a high laser-induced damage threshold is always a significant challenge among these NLO criteria. To balance this relationship, many attempts have been made and resulted in the discovery of a series of high-performance IR NLO crystals, *e.g.*,  $\text{LiGaS}_2$ ,  $\text{Li}_2\text{In}_2\text{SiS}_6$ ,  $\text{Li}_2\text{CdSnS}_4$ ,  $\text{Na}_2\text{ZnGe}_2\text{S}_6$ , and  $\text{BaGa}_2\text{GeQ}_6$  ( $Q = \text{S, Se}$ ). Most of these strategies are mainly focused on using higher electropositive alkali or alkaline-earth cations to substitute the  $\text{Ag}^+$  cations in chalcopyrite-type  $\text{AgGaS}_2$  and  $\text{AgGaSe}_2$  to widen band gaps, while introducing as many as possible NLO-active functional motifs,  $\text{MQ}_4$ , ( $M = \text{Ga, In, Ge, Sn etc.}, Q = \text{S, Se}$ ) to optimize the SHG response.<sup>12–16</sup> Although these attempts are effective and fruitful, they also suffer from some difficulties arising from the fact that ionic and covalent structural units are usually mixed in various assembly processes, whereas the processes favoring good NLO performances can be hardly determined.<sup>17,18</sup>

Based on the study of the structure–property relationship, it is clear that the SHG response mainly depends on NLO-active functional motifs,  $\text{MQ}_4$ , possessing strong covalency. Meanwhile, the 12 *group* transition metal tetrahedra and 13 and 14 *group element* tetrahedra are usually employed as the NLO-active units to generate large SHG responses in compounds.<sup>19–21</sup> Especially for transition metal  $\text{Hg}^{2+}$  cations, they have a heavy atomic mass and highly polarizable characteristics. When they are introduced into chalcogenides, the

Tianjin Key Laboratory of Functional Crystal Materials, Institute of Functional Crystal, College of Materials Science and Engineering, Tianjin University of Technology, Tianjin 300384, China. E-mail: [hwyyu15@gmail.com](mailto:hwyyu15@gmail.com)

† Electronic supplementary information (ESI) available. CCDC 2168297. For ESI and crystallographic data in CIF or other electronic format see DOI: <https://doi.org/10.1039/d2qi00937d>

materials can produce much larger SHG coefficients and a wider IR transparency region than other 12 group transition metals, making the materials highly competitive IR NLO materials, *e.g.*,  $\text{KHg}_4\text{Ga}_5\text{Se}_{12}$  exhibits a large phase-matching SHG response ( $20 \text{ AgGaS}_2$ ).<sup>22</sup> Remarkably, the narrow band gaps of Hg-based compounds, *e.g.*,  $\text{KHg}_4\text{Ga}_5\text{Se}_{12}$  (1.61),  $\text{BaHgSnSe}_4$  (1.98 eV),  $\text{SrHgSnSe}_4$  (2.07 eV),  $\text{Li}_4\text{HgSn}_2\text{Se}_7$  (2.10 eV), and  $\text{SrHgSnS}_4$  (2.72 eV), are unfavorable for them to display a high laser-induced damage threshold.<sup>23,24</sup> In addition, according to Guo's investigation on the electron localization function map,<sup>17</sup> the introduction of strong ionic components has a positive effect on the band gap of the material. Subsequently, it is expected that introducing strongly ionic metal-halogen bonds into Hg-based chalcogenides would be able to increase the band gaps of materials and achieve a good balance between SHG responses and band gaps.<sup>25</sup>

Guided by these ideas, a new Hg-based chalcogenide,  $[\text{Ba}_4\text{Cl}_2][\text{HgGa}_4\text{S}_{10}]$ , has been successfully designed and synthesized by finely mixing three types of chemical bonds with different covalency and ionicity, including covalent Ga-S and Hg-S, and strong ionic Ba-Cl/S bonds. As expected, this compound can exhibit well-balanced IR NLO properties, including a large SHG response ( $1.5 \times \text{AgGaS}_2$ ), wide band gap (2.95 eV), high laser-induced damage threshold ( $15 \times \text{AgGaS}_2$ ), and wide transparent window (0.42–25  $\mu\text{m}$ ). The results demonstrate that fine mixing of covalent and ionic bonds in the structure is an effective approach for achieving the balance between the SHG response and the band gap.

Polycrystalline  $[\text{Ba}_4\text{Cl}_2][\text{HgGa}_4\text{S}_{10}]$  was synthesized through a solid-state reaction in a sealed silicon-tube at 750 °C, and its purity was confirmed by powder X-ray diffraction (Fig. S1†). Then, a millimeter-sized single crystal of  $[\text{Ba}_4\text{Cl}_2][\text{HgGa}_4\text{S}_{10}]$  was grown with  $\text{BaCl}_2$  as the flux. By using these crystals, the structure of  $[\text{Ba}_4\text{Cl}_2][\text{HgGa}_4\text{S}_{10}]$  was determined by single-crystal XRD analysis, which reveals that  $[\text{Ba}_4\text{Cl}_2][\text{HgGa}_4\text{S}_{10}]$  crystallizes in the noncentrosymmetric tetragonal space group,  $I\bar{4}$  (no. 82).<sup>26</sup> The energy-dispersive spectroscopy measurement corroborates the existence of Ba/Cl/Hg/Ga/S with an average atomic ratio of 18.49% : 9.48% : 4.75% : 20.57 : 46.71, which is approximately equal to the theoretical one, 19.05% : 9.52% : 4.76% : 19.05 : 47.62 (Fig. S2†).

The crystal structure of  $[\text{Ba}_4\text{Cl}_2][\text{HgGa}_4\text{S}_{10}]$  is shown in Fig. 1. Its asymmetric unit contains one Ga, one Hg, one Ba, three S, and two Cl atom(s). All the Ga atoms are coordinated by four S atoms to form  $\text{GaS}_4$  tetrahedra with Ga-S distances of 2.244(5)–2.290(5) Å, and every four  $\text{GaS}_4$  tetrahedra connect with each other through corner-sharing to form T2-type  $\text{Ga}_4\text{S}_{10}$  supertetrahedra (Fig. 1a). For Hg atoms, they are also coordinated by four S atoms to form  $\text{HgS}_4$  tetrahedra with a Hg-S distance of 2.548(5) Å, and each  $\text{HgS}_4$  tetrahedron is bonded by four  $\text{Ga}_4\text{S}_{10}$  T2-supertetrahedra through corner-sharing forming a three-dimensional (3D)  $[\text{HgGa}_4\text{S}_{10}]^{6-}$  covalent framework (Fig. 1b). The residual charges of the  $[\text{HgGa}_4\text{S}_{10}]^{6-}$  covalent framework are balanced by a 3D  $[\text{Ba}_4\text{Cl}_2]^{6+}$  guest network, which is composed of the highly distorted  $[\text{Cl}(1)\text{Ba}_4]$

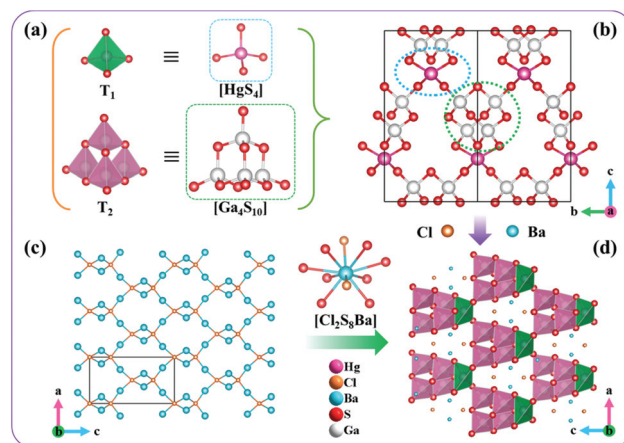


**Fig. 1**  $\text{HgS}_4$  tetrahedron and  $\text{Ga}_4\text{S}_{10}$  T2-supertetrahedron (a). A 3D anionic covalent framework of  $[\text{HgGa}_4\text{S}_{10}]^{6-}$  (b). A 3D  $[\text{Ba}_4\text{Cl}_2]^{6+}$  guest network made of 1D  $[\text{Ba}_4\text{Cl}_2]^{6+}$  chains that are connected alternately by highly distorted  $[\text{Cl}(1)\text{Ba}_4]$  and  $[\text{Cl}(2)\text{Ba}_4]$  building units along the *b* direction (c). A 3D host structure of  $[\text{Ba}_4\text{Cl}_2][\text{HgGa}_4\text{S}_{10}]$  with  $\text{Ba}^{2+}$  cations and  $\text{Cl}^-$  anions residing in the cavities as viewed along the *b*-axis (d).

and  $[\text{Cl}(2)\text{Ba}_4]$  tetrahedra *via* corner- and edge-sharing (Fig. 1c). For Ba-Cl and Ba-S bonds, their bond lengths range from 3.048(1) to 3.107(1) Å and 3.243(5) to 3.644(5) Å, respectively. The bond valence sum calculations resulted in values of 2.01 for  $\text{Ba}^{2+}$ , 2.16 for  $\text{Hg}^{2+}$ , 3.04 for  $\text{Ga}^{3+}$ , 1.95–1.99 for  $\text{S}^{2-}$  and 1.30–1.52 for  $\text{Cl}^-$ .<sup>27</sup> The slightly high oxidation states for  $\text{Cl}^-$  result from the slightly short Ba-Cl bond lengths owing to the extreme difference of electronegativity between Ba and Cl atoms, which is comparable with those of reported chalcogenides, *e.g.*,  $[\text{CsBa}_2\text{Cl}][\text{Ga}_4\text{S}_8]$  and  $[\text{Ba}_4\text{Cl}_2][\text{ZnGa}_4\text{S}_{10}]$ .<sup>28,29</sup> Importantly,  $[\text{Ba}_4\text{Cl}_2][\text{HgGa}_4\text{S}_{10}]$  contains three types of chemical bonds with different covalency and ionicity, including covalent Ga-S and Hg-S, and strong ionic Ba-Cl/S bonds, which is conducive to obtaining well-balanced NLO properties.<sup>30,31</sup>

The UV-vis-NIR diffuse reflectance and absorption spectra of  $[\text{Ba}_4\text{Cl}_2][\text{HgGa}_4\text{S}_{10}]$  are shown in Fig. 2a. It displays a wider band gap (2.95 eV) than those of commercially used  $\text{AgGaS}_2$  (2.70 eV),  $\text{AgGaSe}_2$  (1.83 eV), and  $\text{ZnGeP}_2$  (1.75 eV). Meanwhile,  $[\text{Ba}_4\text{Cl}_2][\text{HgGa}_4\text{S}_{10}]$  contains alkaline-earth  $\text{Ba}^{2+}$  cations without unwanted d-d or f-f electron transitions, the strongly electronegative Cl atom with a blue-shift effect,<sup>6</sup> and an ionic-bonded 3D  $[\text{Ba}_4\text{Cl}_2]^{6+}$  guest network, which contributes to the wide band gap of  $[\text{Ba}_4\text{Cl}_2][\text{HgGa}_4\text{S}_{10}]$ .<sup>17</sup> The wide band gap is positively related to the large laser-induced damage threshold. Furthermore, the laser-induced damage threshold of  $[\text{Ba}_4\text{Cl}_2][\text{HgGa}_4\text{S}_{10}]$  has also been measured based on the single-pulse powder laser-induced damage threshold method with  $\text{AgGaS}_2$  as the reference using a 1064 nm pulse laser (110 A, 1 Hz, 20 ns). The result reveals that  $[\text{Ba}_4\text{Cl}_2][\text{HgGa}_4\text{S}_{10}]$  has a high powder laser-induced damage threshold of 310  $\text{MW cm}^{-2}$ , which is  $\sim 15 \times \text{AgGaS}_2$ . Furthermore, a wide IR transmission region is also essential for the application of NLO crystals. The IR and Raman spectra of  $[\text{Ba}_4\text{Cl}_2][\text{HgGa}_4\text{S}_{10}]$  are

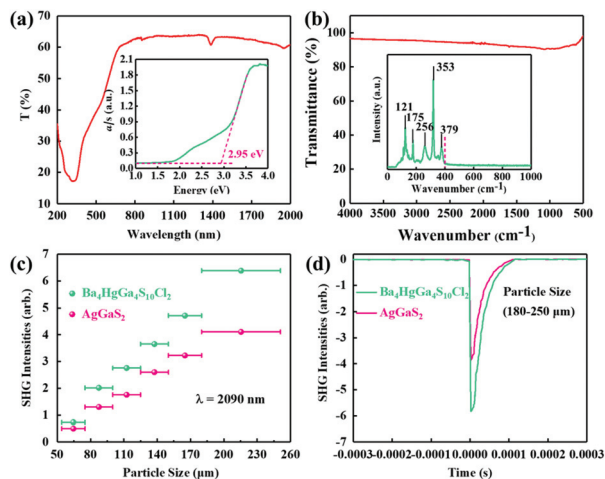


**Fig. 2** The UV-Vis-NIR diffuse reflectance spectrum, inset: band gap (a) and the FTIR spectrum, inset: Raman spectrum (b) of  $[\text{Ba}_4\text{Cl}_2][\text{HgGa}_4\text{S}_{10}]$ . Particle size dependence of the SHG intensities of  $[\text{Ba}_4\text{Cl}_2][\text{HgGa}_4\text{S}_{10}]$  and  $\text{AgGaS}_2$  (c). SHG intensities of  $[\text{Ba}_4\text{Cl}_2][\text{HgGa}_4\text{S}_{10}]$  and AGS at a particle size of 180–250  $\mu\text{m}$  (d).

shown in Fig. 2b. The IR spectrum shows that  $[\text{Ba}_4\text{Cl}_2][\text{HgGa}_4\text{S}_{10}]$  has no obvious absorption in the region of 4000–400  $\text{cm}^{-1}$  (*i.e.*, 2.5–25  $\mu\text{m}$ ), indicating its potential as an IR NLO crystal.<sup>32</sup> The Raman peaks at 353 and 379  $\text{cm}^{-1}$  belong to the characteristic vibrations of the Ga–S bonds. The absorption peak at 256  $\text{cm}^{-1}$  can be assigned to Hg–S bond interactions.

In addition, the low-frequency peaks below 200  $\text{cm}^{-1}$  mainly originate from the Ba–S vibrations. The assignments for the Raman peaks are consistent with those of other chalcogenides, such as  $\text{LiBa}_4\text{Ga}_5\text{S}_{12}$ ,  $(\text{Na}_3\text{Rb})\text{Hg}_2\text{Ge}_2\text{S}_8$  and  $\text{BaHgS}_2$ .<sup>33–35</sup>

As  $[\text{Ba}_4\text{Cl}_2][\text{HgGa}_4\text{S}_{10}]$  crystallizes in the noncentrosymmetric space group of  $I\bar{4}$ , and contains the NLO-active  $[\text{GaS}_4]$  and  $[\text{HgS}_4]$  tetrahedra, a relatively large SHG response could be expected. The powder SHG measurement for  $[\text{Ba}_4\text{Cl}_2][\text{HgGa}_4\text{S}_{10}]$  has been carried out using the modified Kurtz-Perry method under irradiation with a 2090 nm laser with  $\text{AgGaS}_2$  as a reference. As shown in Fig. 2c, the SHG intensity of  $[\text{Ba}_4\text{Cl}_2][\text{HgGa}_4\text{S}_{10}]$  is around  $1.5 \times \text{AgGaS}_2$  at a particle size of 180–250  $\mu\text{m}$  (Fig. 2d). The effective NLO coefficient  $d_{\text{eff}}$  was calculated using the formula  $d_{\text{eff}} = d_{\text{eff,AgGaS}_2} (I_{\text{AgGaS}_2}^{2\omega} / I_{\text{AgGaS}_2}^{\omega})^{1/2}$  (where  $I_{\text{AgGaS}_2}^{2\omega}$  and  $I_{\text{AgGaS}_2}^{\omega}$  are SHG intensities for the sample and  $\text{AgGaS}_2$ , respectively) with polycrystalline  $d_{\text{eff,AgGaS}_2} = 11.8 \text{ pm V}^{-1}$  (polycrystalline  $d_{\text{eff,AgGaS}_2}$  is the angular average of single-crystal  $d_{36, \text{AgGaS}_2} = 13.7 \text{ pm V}^{-1}$ ).<sup>36</sup> Therefore, the experimental polycrystalline  $d_{\text{eff}}$  value is estimated to be  $14.7 \text{ pm V}^{-1}$  for  $[\text{Ba}_4\text{Cl}_2][\text{HgGa}_4\text{S}_{10}]$ . The large SHG response of  $[\text{Ba}_4\text{Cl}_2][\text{HgGa}_4\text{S}_{10}]$  will be conducive to generating a high conversion efficiency in the application.

To understand the origin of the large SHG response in  $[\text{Ba}_4\text{Cl}_2][\text{HgGa}_4\text{S}_{10}]$ , the electron structure of  $[\text{Ba}_4\text{Cl}_2][\text{HgGa}_4\text{S}_{10}]$  has been calculated by first-principles calculations. It shows that  $[\text{Ba}_4\text{Cl}_2][\text{HgGa}_4\text{S}_{10}]$  has a direct band

gap of 2.53 eV (Fig. S3<sup>†</sup>), which is smaller than the experimental value attributable to the discontinuity of exchange–correlation energy.<sup>37</sup> The electronic densities of states (DOS) of  $[\text{Ba}_4\text{Cl}_2][\text{HgGa}_4\text{S}_{10}]$  are shown in Fig. S4.<sup>†</sup> It is clear that the tops of the valence bands of  $[\text{Ba}_4\text{Cl}_2][\text{HgGa}_4\text{S}_{10}]$  are mainly composed of S 3p states with a small part of the Ga 4p and Cl 3p states, while the bottoms of the conduction bands are primarily S 3p, Ga 4s, Ga 4p, Hg 6s and Ba 5d states. These results indicate that the  $[\text{HgGa}_4\text{S}_{10}]^{6-}$  anionic moiety has the main contribution to the band gap and SHG response of  $[\text{Ba}_4\text{Cl}_2][\text{HgGa}_4\text{S}_{10}]$ . In order to further understand the contribution, an intrinsic dipole moment calculation was implemented by a simple bond valence model.<sup>38</sup> The calculated results are listed in Table S1.<sup>†</sup> The dipole moments from  $\text{GaS}_4$  and  $\text{HgS}_4$  tetrahedra are 2.99 and zero Debye (D), respectively. Although the static dipole moment of  $\text{HgS}_4$  units in the unit cell is zero, introducing  $\text{Hg}^{2+}$  in  $[\text{Ba}_4\text{Cl}_2][\text{HgGa}_4\text{S}_{10}]$  increases the dipole moment in  $\text{Ga}_4\text{S}_{10}$  supertetrahedra, which is systematically larger than those in  $[\text{RbBa}_2\text{Cl}][\text{Ga}_4\text{S}_8]$ ,<sup>28</sup>  $[\text{Ba}_4\text{Cl}_2][\text{ZnGa}_4\text{S}_{10}]$ ,<sup>29</sup>  $[\text{KBa}_3\text{Cl}_2][\text{Ga}_5\text{Se}_{10}]$ ,<sup>39</sup> and  $[\text{Ba}_4\text{Cl}_2][\text{MGa}_4\text{Se}_{10}]$  ( $M = \text{Zn}, \text{Cd}$ ).<sup>40</sup> Additionally, the induced dipole moments from the  $\text{MQ}_4$  ( $M = \text{Zn}, \text{Ga}, \text{Hg}$  and  $Q = \text{S}, \text{Se}$ ) units in  $\text{AgGaS}_2$ ,  $\text{AgGaSe}_2$ ,  $\text{Ba}_3\text{KGa}_5\text{Se}_{10}\text{Cl}_2$ ,  $\text{Ba}_2\text{RbGa}_4\text{S}_8\text{Cl}$ ,  $\text{Ba}_4\text{ZnGa}_4\text{S}_{10}\text{Cl}_2$ ,  $\text{Ba}_4\text{ZnGa}_4\text{Se}_{10}\text{Cl}_2$ , and  $[\text{Ba}_4\text{Cl}_2][\text{HgGa}_4\text{S}_{10}]$  were also quantified based on the calculation of the empirical “flexibility index”  $F$ .<sup>28,29,39–43</sup> As listed in Table 1, the  $F$  value of the  $[\text{HgS}_4]$  unit in  $[\text{Ba}_4\text{Cl}_2][\text{HgGa}_4\text{S}_{10}]$  is slightly larger than those of the  $\text{MQ}_4$  ( $M = \text{Zn}, \text{Ga}$  and  $Q = \text{S}, \text{Se}$ ) units in other chalcogenides, *e.g.*,  $\text{AgGaS}_2$ ,  $\text{Ba}_2\text{RbGa}_4\text{S}_8\text{Cl}$  and  $\text{Ba}_4\text{ZnGa}_4\text{S}_{10}\text{Cl}_2$ . The relatively large induced dipole moment is helpful for  $[\text{Ba}_4\text{Cl}_2][\text{HgGa}_4\text{S}_{10}]$  to generate an enhanced SHG response. In addition, the NLO coefficients of  $[\text{Ba}_4\text{Cl}_2][\text{HgGa}_4\text{S}_{10}]$  can also be calculated based on the calculated electron structure. According to Kleinman symmetry,  $[\text{Ba}_4\text{Cl}_2][\text{HgGa}_4\text{S}_{10}]$  has two nonzero independent SHG coefficients,  $d_{15} = d_{31} = 9.40 \text{ pm V}^{-1}$  and  $d_{14} = d_{36} = 22.04 \text{ pm V}^{-1}$ . Obviously, the calculated  $d_{36}$  value is about 1.6 times that of  $\text{AgGaS}_2$  ( $d_{36, \text{AgGaS}_2} = 13.70 \text{ pm V}^{-1}$ ),<sup>18</sup> which is also matched with the experimental result.

**Table 1** The space groups, SHG responses, and flexibility indices ( $F$ ) of  $\text{MQ}_4$  ( $M = \text{Ga}, \text{Zn}, \text{Hg}$  and  $Q = \text{S}, \text{Se}$ ) units in  $\text{AgGaS}_2$ ,  $\text{AgGaSe}_2$ ,  $\text{Ba}_3\text{KGa}_5\text{Se}_{10}\text{Cl}_2$ ,  $\text{Ba}_2\text{RbGa}_4\text{S}_8\text{Cl}$ ,  $\text{Ba}_4\text{ZnGa}_4\text{S}_{10}\text{Cl}_2$ ,  $\text{Ba}_4\text{ZnGa}_4\text{Se}_{10}\text{Cl}_2$ ,  $\text{Ba}_4\text{HgGa}_4\text{S}_{10}\text{Cl}_2$ , and  $[\text{Ba}_4\text{Cl}_2][\text{HgGa}_4\text{S}_{10}]$

Compounds	Space groups	$\text{MQ}_4$ units	$d_{ij}$ ( $\times \text{AGS}$ , $\text{pm V}^{-1}$ )	$F$	Ref.
$\text{AgGaS}_2$	$I\bar{4}2d$	$\text{GaS}_4$	$d_{36} = 13.4$	0.212	41
$\text{AgGaSe}_2$	$I\bar{4}2d$	$\text{GaSe}_4$	$d_{36} = 33.0$	0.211	42
$\text{Ba}_3\text{KGa}_5\text{Se}_{10}\text{Cl}_2$	$I\bar{4}$	$\text{GaSe}_4$	$3.6 \times \text{AGS}$	0.258	39
$\text{Ba}_2\text{RbGa}_4\text{S}_8\text{Cl}$	$Pmn2_1$	$\text{GaS}_4$	$0.9 \times \text{AGS}$	0.220–0.236	28
$\text{Ba}_4\text{ZnGa}_4\text{S}_{10}\text{Cl}_2$	$I\bar{4}$	$\text{GaS}_4$	$1.1 \times \text{AGS}$	0.183–0.223	29
$\text{Ba}_4\text{ZnGa}_4\text{Se}_{10}\text{Cl}_2$	$I\bar{4}$	$\text{ZnS}_4$	$1.6 \times \text{AGS}$	0.212–0.255	40
		$\text{GaSe}_4$			
$[\text{Ba}_4\text{Cl}_2][\text{HgGa}_4\text{S}_{10}]$	$I\bar{4}$	$\text{GaS}_4$ $\text{HgS}_4$	$1.5 \times \text{AGS}$	0.226–0.235	

Clearly,  $[\text{Ba}_4\text{Cl}_2][\text{HgGa}_4\text{S}_{10}]$  can exhibit a relatively large SHG response and a wide band gap, which would be related to the covalent  $[\text{HgGa}_4\text{S}_{10}]^{6-}$  anionic moiety and the ionic  $[\text{Ba}_4\text{Cl}_2]^{6+}$  cation network, respectively.<sup>18,29,43–45</sup> To better show the different covalence and ionicity, we also calculated the overlap populations and electron localization function (ELF) of  $[\text{Ba}_4\text{Cl}_2][\text{HgGa}_4\text{S}_{10}]$  based on first-principles calculations. Given that the overlap populations can represent different electron density localization statuses, *i.e.*, the larger values ( $>0.5$ ) reflect the localized electron states and the stronger covalent characteristics; inversely, the smaller values ( $<0.5$ ) represent delocalized electron states and the stronger ionic characteristics.<sup>18</sup> As shown in Fig. 3a, it can be seen that the Ga/Hg–S bonds (0.45–0.66 e) show strong covalency and Ba–S/Cl bonds (0.1–0.13 e) exhibit strong ionicity in  $[\text{Ba}_4\text{Cl}_2][\text{HgGa}_4\text{S}_{10}]$ . Furthermore, the ELF map of  $[\text{Ba}_4\text{Cl}_2][\text{HgGa}_4\text{S}_{10}]$  reveals that the covalent Ga/Hg–S and strong ionic Ba–S/Cl bonds present fine mixing in the structure (Fig. 3b), which achieves the expected balance between the SHG response and the band gap in  $[\text{Ba}_4\text{Cl}_2][\text{HgGa}_4\text{S}_{10}]$ .

To further understand the importance of  $[\text{Ba}_4\text{Cl}_2][\text{HgGa}_4\text{S}_{10}]$  with fine mixing of covalency and ionicity for exploring IR NLO crystals, a property comparison between  $[\text{Ba}_4\text{Cl}_2][\text{HgGa}_4\text{S}_{10}]$  and some high-performance IR NLO crystals with Hg-based and Ga–S bonds has been performed. Compared to the recently reported Hg-based compounds (*e.g.*,  $(\text{Hg}_6\text{P}_3)(\text{In}_2\text{Cl}_9)$  ( $d_{ij} = 0.5 \times \text{AgGaS}_2$ ,  $E_g = 3.13$  eV),<sup>46</sup>  $(\text{Hg}_2\text{Cd}_2\text{S}_2\text{Br})\text{Br}$  ( $E_g = 2.41$  eV),<sup>47</sup>  $(\text{Hg}_3\text{Se}_2)(\text{Se}_2\text{O}_5)$  ( $E_g = 2.63$  eV),<sup>48</sup>  $\text{KHg}_4\text{Ga}_5\text{Se}_{12}$  ( $d_{ij} = 20 \times \text{AgGaS}_2$ ,  $E_g = 1.61$  eV),<sup>22</sup>  $\text{SrHgSnS}_4$  ( $d_{ij} = 1.9 \times \text{AgGaS}_2$ ,  $E_g = 2.72$  eV)<sup>23</sup>), and chalcogenides with Ga–S bonds (*e.g.*,  $\text{Ba}_2\text{Ga}_8\text{GeS}_{16}$  ( $d_{ij} = 1 \times \text{AgGaS}_2$ ,  $E_g = 3.0$  eV)<sup>49</sup> and  $\text{Ga}_2\text{S}_3$  ( $d_{ij} = 0.2 \times \text{AgGaS}_2$ ,  $E_g = 2.8$  eV)<sup>50</sup>),  $[\text{Ba}_4\text{Cl}_2][\text{HgGa}_4\text{S}_{10}]$  constructed from the structural units with mixing of covalency (Hg–S and Ga–S bonds) and ionicity (Ba–Cl/S bond) can exhibit a good comprehensive IR NLO performance ( $d_{ij} = 1.5 \times \text{AgGaS}_2$  and  $E_g = 2.95$  eV). Additionally, compared to  $\text{AgGaS}_2$  and other chalcohalides,  $[\text{Ba}_4\text{Cl}_2][\text{HgGa}_4\text{S}_{10}]$  exhibits a relatively large SHG response, wide band gap, and high laser-induced damage threshold (Fig. S5 and Table S2†), which achieves the expected balance between the SHG response and the band gap. These results indicate that  $[\text{Ba}_4\text{Cl}_2][\text{HgGa}_4\text{S}_{10}]$  will be a promising IR NLO crystal, and the Hg-based chalcohalides with mixed covalent and ionic bonds

may be a worthwhile materials class for the exploration of IR NLO crystals.

In conclusion, a new noncentrosymmetric chalcohalide,  $[\text{Ba}_4\text{Cl}_2][\text{HgGa}_4\text{S}_{10}]$ , has been successfully synthesized by introducing electronegative halogens in a Hg-based chalcogenide. Its structure consists of a 3D  $[\text{HgGa}_4\text{S}_{10}]^{6-}$  anionic moiety formed by corner-sharing tetrahedral  $\text{HgS}_4$  (T1) and supertetrahedral  $\text{Ga}_4\text{S}_{10}$  clusters (T2), as well as a 3D  $[\text{Ba}_4\text{Cl}_2]^{6+}$  cation network. The property measurements show that it can exhibit balanced NLO properties, including a large SHG response ( $1.5 \times \text{AgGaS}_2$  at 2090 nm), wide band gap (2.95 eV), high laser-induced damage threshold ( $15 \times \text{AgGaS}_2$ ), and wide transparent window (0.42–25  $\mu\text{m}$ ). These results show that  $[\text{Ba}_4\text{Cl}_2][\text{HgGa}_4\text{S}_{10}]$  would be a promising IR NLO crystal. Furthermore, the overlap populations and ELF map analysis results confirm that the balanced NLO properties of  $[\text{Ba}_4\text{Cl}_2][\text{HgGa}_4\text{S}_{10}]$  mainly originate from the fine mixing of covalency and ionicity in the structure. This work will provide a feasible way for exploring excellent IR NLO crystals through finely mixing covalency and ionicity.

## Author contributions

Y. Z. performed the experiments, data analysis, theoretical calculations, and paper writing. H. W. designed and supervised the experiments. H. Y. provided major revisions of the manuscript. Z. H. supervised the optical experiments. J. W. and Y. W. helped with the analyses of the crystallization process and the data. All the authors discussed the results and commented on the manuscript.

## Conflicts of interest

There are no conflicts to declare.

## Acknowledgements

This work was supported by the National Natural Science Foundation of China (Grant No. 22071179, 52172006, 51972230, 51890864, 61835014, and 51890865) and the Natural Science Foundation of Tianjin (Grant No. 20JCQJC00060, and 21JCQJC00090).

## Notes and references

- 1 Y. Tang, K. Li, X. Zhang, J. Deng, G. Li and E. Brasselet, Harmonic spin-orbit angular momentum cascade in nonlinear optical crystals, *Nat. Photonics*, 2020, **14**, 658–662.
- 2 D. Cyranoski, Materials science: China's crystal cache, *Nature*, 2009, **457**, 953–955.
- 3 H. Wu, H. Yu, Z. Yang, X. Hou, X. Su, S. Pan, K. Poeppelmeier and J. Rondinelli, Designing a Deep-Ultraviolet Nonlinear Optical Material with a Large Second

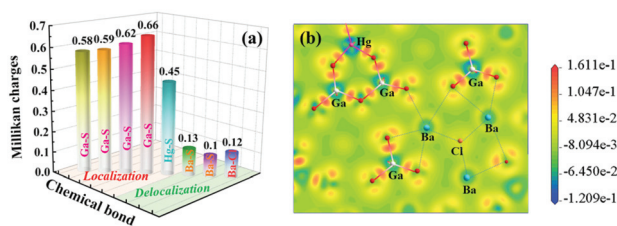


Fig. 3 Overlap populations (a) and electron localization function (b) of  $[\text{Ba}_4\text{Cl}_2][\text{HgGa}_4\text{S}_{10}]$ .

- Harmonic Generation Response, *J. Am. Chem. Soc.*, 2013, **135**, 4215–4218.
- 4 X. Wang, Y. Wang, B. Zhang, F. Zhang, Z. Yang and S. Pan, CsB<sub>4</sub>O<sub>6</sub>F: A Congruent-Melting Deep-Ultraviolet Nonlinear Optical Material by Combining Superior Functional Units, *Angew. Chem., Int. Ed.*, 2017, **56**, 14119–14123.
  - 5 G. Shi, Y. Wang, F. Zhang, B. Zhang, Z. Yang, X. Hou, S. Pan and K. Poeppelmeier, Finding the Next Deep-Ultraviolet Nonlinear Optical Material: NH<sub>4</sub>B<sub>4</sub>O<sub>6</sub>F, *J. Am. Chem. Soc.*, 2017, **139**, 10645–10648.
  - 6 Y. Wang, B. Zhang, Z. Yang and S. Pan, Cation-Tuned Synthesis of Fluorooxoborates: Towards Optimal Deep-Ultraviolet Nonlinear Optical Materials, *Angew. Chem., Int. Ed.*, 2018, **57**, 2150–2154.
  - 7 J. Chen, H. Chen, F. Xu, L. Cao, X. Jiang, S. Yang, Y. Sun, X. Zhao, C. Lin and N. Ye, Mg<sub>2</sub>In<sub>3</sub>Si<sub>2</sub>P<sub>7</sub>: A Quaternary Diamond-like Phosphide Infrared Nonlinear Optical Material Derived from ZnGeP<sub>2</sub>, *J. Am. Chem. Soc.*, 2021, **143**, 10309–10316.
  - 8 P. Budni, L. Pomeranz, M. Lemons, C. Miller, J. Mosto and E. Chicklis, Efficient mid-infrared laser using 1.9- $\mu$ m-pumped Ho:YAG and ZnGeP<sub>2</sub> optical parametric oscillators, *J. Opt. Soc. Am. B*, 2000, **17**, 723–728.
  - 9 A. Harasaki and K. Kato, New Data on the Nonlinear Optical Constant, Phase-Matching, and Optical Damage of AgGaS<sub>2</sub>, *Jpn. J. Appl. Phys.*, 1997, **36**, 700–703.
  - 10 G. Catella, L. Shiozawa, J. Hietanen, R. Eckardt, R. Route, R. Feigelson, D. Cooper and C. Marquardt, Mid-IR absorption in AgGaSe<sub>2</sub> optical parametric oscillator crystals, *Appl. Opt.*, 1993, **32**, 3948–3951.
  - 11 A. Jackson, M. Ohmer and S. LeClair, Relationship of the second order nonlinear optical coefficient to energy gap in inorganic non-centrosymmetric crystals, *Infrared Phys. Technol.*, 1997, **38**, 233–244.
  - 12 W. Yin, K. Feng, W. Hao, J. Yao and Y. Wu, Synthesis, Structure, and Properties of Li<sub>2</sub>In<sub>2</sub>MQ<sub>6</sub> (M = Si, Ge; Q = S, Se): A New Series of IR Nonlinear Optical Materials, *Inorg. Chem.*, 2012, **51**, 5839–5843.
  - 13 V. Petrov, A. Yelisseyev, L. Isaenko, S. Lobanov and J. Zondy, Second harmonic generation and optical parametric amplification in the mid-IR with orthorhombic biaxial crystals LiGaS<sub>2</sub> and LiGaSe<sub>2</sub>, *Appl. Phys. B*, 2004, **78**, 543–546.
  - 14 J. Lekse, M. Moreau, K. McNerny, J. Yeon, P. Halasyamani and J. Aitken, Second-Harmonic Generation and Crystal Structure of the Diamond-like Semiconductors Li<sub>2</sub>CdGeS<sub>4</sub> and Li<sub>2</sub>CdSnS<sub>4</sub>, *Inorg. Chem.*, 2009, **48**, 7516–7518.
  - 15 B. Zhang, G. Shi, Z. Yang, F. Zhang and S. Pan, Fluorooxoborates: Beryllium-Free Deep-Ultraviolet Nonlinear Optical Materials without Layered Growth, *Angew. Chem., Int. Ed.*, 2017, **56**, 3916–3919.
  - 16 S. Grechin, P. Nikolaev, A. Ionin, I. Kinyaevskii and Y. Andreev, BaGa<sub>2</sub>GeS<sub>6</sub> and BaGa<sub>2</sub>GeSe<sub>6</sub> crystals for non-linear optical frequency conversion, *Quantum Electron.*, 2020, **50**, 782–787.
  - 17 X. Jiang, S. Lin, C. He, B. Liu and G. Guo, Uncovering a Functional Motif of Nonlinear Optical Materials by In Situ Electron Density and Wavefunction Studies Under Laser Irradiation, *Angew. Chem., Int. Ed.*, 2021, **60**, 11799–11803.
  - 18 B. Liu, X. Jiang, S. Pei, W. Chen, L. Yang and G. Guo, Balanced infrared nonlinear optical performance achieved by modulating the covalency and ionicity distributions in the electron localization function map, *Mater. Horiz.*, 2021, **8**, 3394–3398.
  - 19 X. Dong, Q. Jing, Y. Shi, Z. Yang, S. Pan, K. Poeppelmeier, J. Young and J. Rondinelli, Pb<sub>2</sub>Ba<sub>3</sub>(BO<sub>3</sub>)<sub>3</sub>Cl: A Material with Large SHG Enhancement Activated by Pb-Chelated BO<sub>3</sub> Groups, *J. Am. Chem. Soc.*, 2015, **137**, 9417–9422.
  - 20 H. Lin, W. Wei, H. Chen, X. Wu and Q. Zhu, Rational design of infrared nonlinear optical chalcogenides by chemical substitution, *Coord. Chem. Rev.*, 2020, **406**, 213150.
  - 21 S. Guo, Y. Chi and G. Guo, Recent achievements on middle and far-infrared second-order nonlinear optical materials, *Coord. Chem. Rev.*, 2017, **335**, 44–57.
  - 22 M. Zhou, Y. Yang, Y. Guo, Z. Lin, J. Yao, Y. Wu and C. Chen, Hg-Based Infrared Nonlinear Optical Material KHg<sub>4</sub>Ga<sub>5</sub>Se<sub>12</sub> Exhibits Good Phase-Matchability and Exceptional Second Harmonic Generation Response, *Chem. Mater.*, 2017, **29**, 7993–8002.
  - 23 Y. Guo, F. Liang, Z. Li, W. Xing, Z. Lin, J. Yao, A. Mar and Y. Wu, AHgSnQ<sub>4</sub> (A = Sr, Ba; Q = S, Se): A Series of Hg-Based Infrared Nonlinear-Optical Materials with Strong Second-Harmonic-Generation Response and Good Phase Matchability, *Inorg. Chem.*, 2019, **58**, 10390–10398.
  - 24 Y. Guo, F. Liang, Z. Li, W. Xing, Z. Lin, J. Yao and Y. Wu, Li<sub>4</sub>HgSn<sub>2</sub>Se<sub>7</sub>: The First Second-Order Nonlinear Optical-Active Selenide in the I<sub>4</sub>-II-IV<sub>2</sub>-VI<sub>7</sub> Diamond-like Family, *Cryst. Growth Des.*, 2019, **19**, 5494–5497.
  - 25 Q. Yue, W. Wei, H. Chen, X. Wu, H. Lin and Q. Zhu, Salt-inclusion chalcogenides: an emerging class of IR nonlinear optical materials, *Dalton Trans.*, 2020, **49**, 14338–14343.
  - 26 Crystal data of [Ba<sub>4</sub>Cl<sub>2</sub>][HgGa<sub>4</sub>S<sub>10</sub>]:  $a = 8.308(2)$  Å,  $b = 8.308(2)$  Å,  $c = 15.272(4)$  Å,  $\alpha = \beta = \gamma = 90^\circ$ ,  $V = 1054.0(7)$  Å<sup>3</sup>. Numbers 2168297 (for [Ba<sub>4</sub>Cl<sub>2</sub>][HgGa<sub>4</sub>S<sub>10</sub>]) contain the supplementary crystallographic data for this paper.
  - 27 I. Brown and D. Altermatt, Bond-valence parameters obtained from a systematic analysis of the Inorganic Crystal Structure Database, *Acta Crystallogr.*, 2010, **41**, 244–247.
  - 28 B. Liu, X. Jiang, H. Zeng and G. C. Guo, [ABa<sub>2</sub>Cl][Ga<sub>4</sub>S<sub>8</sub>] (A = Rb, Cs): Wide-Spectrum Nonlinear Optical Materials Obtained by Polycation-Substitution-Induced Nonlinear Optical (NLO)-Functional Motif Ordering, *J. Am. Chem. Soc.*, 2020, **142**, 10641–10645.
  - 29 H. Chen, Y. Li, B. Li, P. Liu, H. Lin, Q. Zhu and X. Wu, Salt-Inclusion Chalcogenide [Ba<sub>4</sub>Cl<sub>2</sub>][ZnGa<sub>4</sub>S<sub>10</sub>]: Rational Design of an IR Nonlinear Optical Material with Superior Comprehensive Performance Derived from AgGaS<sub>2</sub>, *Chem. Mater.*, 2020, **32**, 8012–8019.

- 30 L. Lin, X. Jiang, C. Wu, Z. Lin, Z. Huang, M. Humphrey and C. Zhang, CsZrF<sub>4</sub>(IO<sub>3</sub>): The First Polar Zirconium Iodate with cis-[ZrO<sub>2</sub>F<sub>6</sub>] Polyhedra Inducing Optimized Balance of Large Band Gap and Second Harmonic Generation, *Chem. Mater.*, 2021, **33**, 5555–5562.
- 31 J. Zhang, D. Clark, J. Brant, K. Rosmus, P. Grima, J. Lekse, J. Jang and J. Aitken,  $\alpha$ -Li<sub>2</sub>ZnGeS<sub>4</sub>: A Wide-Bandgap Diamond-like Semiconductor with Excellent Balance between Laser-Induced Damage Threshold and Second Harmonic Generation Response, *Chem. Mater.*, 2020, **32**, 8947–8955.
- 32 D. Clark, J. Zhang, A. Craig, A. Weiland, J. Brant, J. Cho, Y. Kim, J. Jang and J. Aitken, The Kurtz-Perry powder technique revisited: A case study on the importance of reference quality and broadband nonlinear optical measurements using LiInSe<sub>2</sub>, *J. Alloys Compd.*, 2022, **917**, 165381.
- 33 K. Wu, X. Su, S. Pan and Z. Yang, Synthesis and characterization of mid-infrared transparency compounds: acentric BaHgS<sub>2</sub> and centric Ba<sub>8</sub>Hg<sub>4</sub>S<sub>5</sub>Se<sub>7</sub>, *Inorg. Chem.*, 2015, **54**, 2772–2779.
- 34 C. Tang, W. Xing, F. Liang, M. Sun, J. Tang, Z. Lin, J. Yao, K. Chen, J. Wu, W. Yin and K. Bin, Structural Modification from Centrosymmetric Rb<sub>4</sub>Hg<sub>2</sub>Ge<sub>2</sub>S<sub>8</sub> to Noncentrosymmetric (Na<sub>3</sub>Rb)Hg<sub>2</sub>Ge<sub>2</sub>S<sub>8</sub>: Mixed Alkali-metals Strategy for Infrared Nonlinear Optical Material Design, *J. Mater. Chem. C*, 2022, **10**, 3300–3306.
- 35 A. Abudurusuli, J. Li, T. Tong, Z. Yang and S. Pan, LiBa<sub>4</sub>Ga<sub>5</sub>Q<sub>12</sub> (Q = S, Se): Noncentrosymmetric Metal Chalcogenides with a Cesium Chloride Topological Structure Displaying a Remarkable Laser Damage Threshold, *Inorg. Chem.*, 2020, **59**, 5674–5682.
- 36 B. Liu, H. Zeng, X. Jiang and G. Guo, Phase Matching Achieved by Bandgap Widening in Infrared Nonlinear Optical Materials [ABa<sub>3</sub>Cl<sub>2</sub>][Ga<sub>5</sub>S<sub>10</sub>] (A = K, Rb, and Cs), *CCS Chem.*, 2021, **3**, 964–973.
- 37 R. Godby, M. Schlüter and L. Sham, Trends in self-energy operators and their corresponding exchange-correlation potentials, *Phys. Rev. B: Condens. Matter Mater. Phys.*, 1987, **36**, 6497–6500.
- 38 I. Brown, Recent Developments in the Methods and Applications of the Bond Valence Model, *Chem. Rev.*, 2009, **109**, 6858–6919.
- 39 P. Yu, L. Zhou and L. Chen, Noncentrosymmetric inorganic open-framework chalcogenides with strong middle IR SHG and red emission: Ba<sub>3</sub>AGa<sub>5</sub>Se<sub>10</sub>Cl<sub>2</sub> (A = Cs, Rb, K), *J. Am. Chem. Soc.*, 2012, **134**, 2227–2235.
- 40 Y. Li, P. Liu, L. Hu, L. Chen, H. Lin, L. Zhou and L. Wu, Strong IR NLO Material Ba<sub>4</sub>MGa<sub>4</sub>Se<sub>10</sub>Cl<sub>2</sub>: Highly Improved Laser Damage Threshold via Dual Ion Substitution Synergy, *Adv. Opt. Mater.*, 2015, **3**, 957–966.
- 41 A. Okorogu, S. Mirov, W. Lee, D. Crouthamel, N. Jenkins, A. Dergachev, K. Vodopyanov and V. Badikov, Tunable middle infrared downconversion in GaSe and AgGaS<sub>2</sub>, *Opt. Commun.*, 1998, **155**, 307–312.
- 42 G. Boyd, H. Kasper, J. McFee and F. Storz, Linear and non-linear optical properties of some ternary selenides, *IEEE J. Quantum Electron.*, 1972, **8**, 900–908.
- 43 X. Jiang, S. Zhao, Z. Lin, J. Luo, P. Bristowe, X. Guan and C. Chen, The role of dipole moment in determining the nonlinear optical behavior of materials: ab initio studies on quaternary molybdenum tellurite crystals, *J. Mater. Chem. C*, 2014, **2**, 530–537.
- 44 X. Jiang, S. Deng, M. Whangbo and G. Guo, Material research from the viewpoint of functional motifs, *Natl. Sci. Rev.*, 2022, nwac017.
- 45 J. Chen, Q. Wu, H. Tian, X. Jiang, F. Xu, X. Zhao, Z. Lin, M. Luo and N. Ye, Uncovering a Vital Band Gap Mechanism of Pnictides, *Adv. Sci.*, 2022, **9**, 2105787.
- 46 X. Jiang, M. Zhang, H. Zeng, G. Guo and J. Huang, Inorganic Supramolecular Compounds with 3-D Chiral Frameworks Show Potential as Both Mid-IR Second-Order Nonlinear Optical and Piezoelectric Materials, *J. Am. Chem. Soc.*, 2011, **133**, 3410–3418.
- 47 J. Zou, Q. Peng, S. Luo, X. Tang, A. Zhang, G. Zeng and G. Guo, Synthesis, crystal and band structures, and optical properties of a novel quaternary mercury and cadmium chalcogenidehalide: (Hg<sub>2</sub>Cd<sub>2</sub>S<sub>2</sub>Br)Br, *CrystEngComm*, 2011, **13**, 3862–3867.
- 48 J. Zou, G. Guo, S. Guo, Y. Lu, K. Wu, M. Wang and J. Huang, Synthesis, crystal and band structures, and optical properties of a new mixed-framework mercury selenide diselenite, (Hg<sub>3</sub>Se<sub>2</sub>)(Se<sub>2</sub>O<sub>5</sub>), *Dalton Trans.*, 2007, 4854–4858.
- 49 B. Liu, H. Zeng, M. Zhang, Y. Fan, G. Guo, J. Huang and Z. Dong, Syntheses, Structures, and Nonlinear-Optical Properties of Metal Sulfides Ba<sub>2</sub>Ga<sub>8</sub>MS<sub>16</sub> (M = Si, Ge), *Inorg. Chem.*, 2015, **54**, 976–981.
- 50 M. Zhang, X. Jiang, L. Zhou and G. Guo, Two phases of Ga<sub>2</sub>S<sub>3</sub>: promising infrared second-order nonlinear optical materials with very high laser induced damage thresholds, *J. Mater. Chem. C*, 2013, **1**, 4754–4760.